Supplementary files

High piezoelectricity induced by lattice distortion and domain realignment in Li$_2$CO$_3$-added lead-based ceramics

Hao Chen, Yining Xie, Jingwen Xi, Wanfeng Zhuang, Weiling Wang, Jie Xing, Hong Liu*, Jianguo Zhu

College of Materials Science and Engineering, Sichuan University, Chengdu 610064, Sichuan, China

*Corresponding author. E-mail address: liuh@scu.edu.cn (H. Liu)

Experimental procedure

Sample Preparation

The ceramics were prepared by the traditional solid-state reaction route. The oxides including PbO (99%), NiO (98%), Nb$_2$O$_5$ (99.5%), ZnO (99%), ZrO$_2$ (99%), TiO$_2$ (98%), Li$_2$CO$_3$ (98%) were mixed in a ball mill jar with anhydrous ethanol for 12 h. The powders were dried and then calcined at 780 °C for 2 h. The calcined powders were milled again for 12 h. After drying, the powders were pressed into disks with a thickness of 1 mm and a diameter of 10 mm with 5 % Polyvinyl alcohol (PVA) as binder at 490 MPa. After burning at 550 °C for 4 h to remove the PVA, the disks were sintered at 1020 °C for 2 h. The ceramics were poled by 2 kV/mm DC voltage in 120 °C silicone oil.

Characterization of microstructure and electrical properties

The crystal and phase structures were analyzed by X-ray diffraction (XRD) (X'Pert Pro MPD instrument, B.V. PANalytical, Netherlands) and Raman

Spectrometer (LabRAM HR, HORIBA France). The surface morphology was observed by scanning electron microscopy (SEM, S-3400N, HITACHI, Japan). High-angle annular dark-field (STEM–HAADF) images were obtained using high-resolution scanning transmission electron microscopy (Spectra 300S/TEM, Thermo Fisher Scientific, USA). The piezoelectric constant (d_{33}) was determined through a quasi-static piezoelectric constant meter (ZJ-3A, Institute of Acoustics, Chinese Academy of Sciences, China). The domain structures were observed by piezoelectric force microscopy (PFM) (Asylum Research, MFP-3D, USA). The dielectric properties were determined by impedance analyzers (HP 4294A, Agilent, USA). The ferroelectric P–E hysteresis loops were measured by a ferroelectric tester (Radiant Technologies, Median, New York, USA).
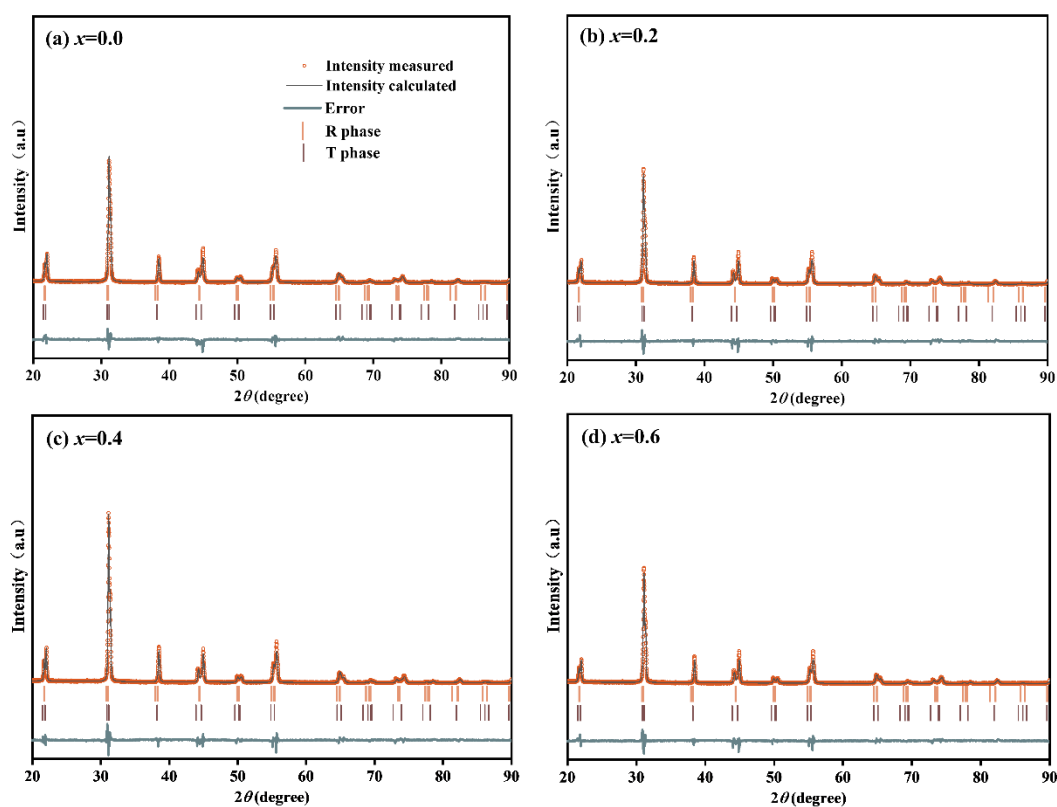

Fig. S1 (a-d) Rietveld refinement of the XRD patterns of the xLi-PNNZNZT.

With increasing Li$^+$ ion content, the six vibration modes tend to shift towards the high frequency, indicating that the structure of the [BO$_6$] octahedron is affected by the substitution of Li$^+$ ions for Pb^{2+} ions, which is consistent with the Rietveld refined results in Table S1. Fig. S2 illustrates the Raman spectra of the xLi-PNNZNZT according to the following formula[1]:

$$\omega = \sqrt{\alpha/\mu} \tag{S1}$$

where μ is the reduced mass, ω and α represent the vibration mode frequency and the force constant, respectively. The substitution of Pb^{2+} with an ionic radius of 1.49 Å by small Li$^+$ with an ionic radius of 1.24 Å results in a reduction of the cell volume and lattice shrinkage, which leads to an increase in the force constant of the [BO$_6$] octahedron, shifting the Raman frequency peaks to a higher band.
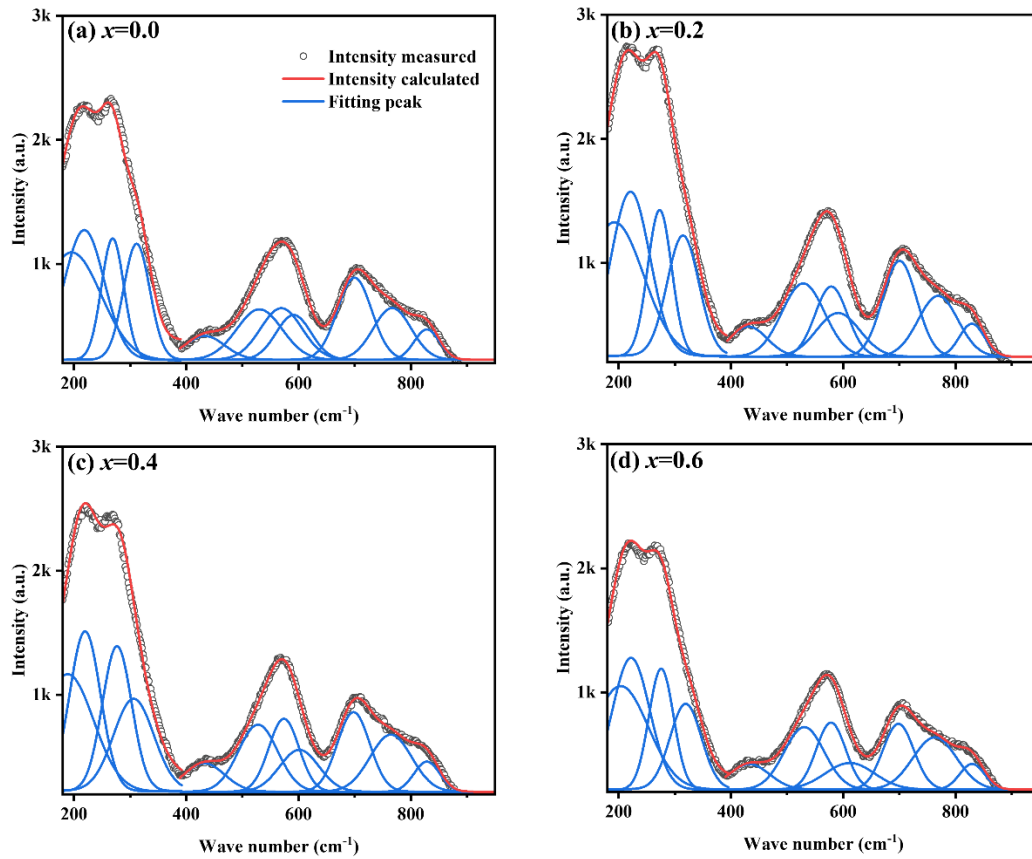
Fig. S2 (a-d) Raman spectra of the xLi-PNNZNZT.

Fig. S3a shows the temperature-dependent dielectric constant (ε_r) at different frequencies. The permittivity peaks shift to higher temperatures with increasing frequency, which means the xLi-PNNZNZT are a typical relaxor ferroelectric. The Li$^+$-ion doping can improve the Curie temperature (T_C), which increases from 253 °C at x=0.0 to 269 °C at x=0.4 (Fig. S3b). For ferroelectric materials, the ε_r needs to follow the Curie-Weiss law when the temperature is above T_C[2]:

$$\varepsilon = C/(T-T_0) \tag{S2}$$

where C and T_0 represent the Curie-Weiss constant and the Curie-Weiss temperature, respectively, which can be obtained by linear fitting the data in Fig. S3b. The degree of deviation from the Curie-Weiss law is expressed as[3, 4]:

$$\Delta T_m = T_{cw} - T_m \tag{S3}$$

where T_m is the temperature at maximum permittivity and T_{cw} denotes the temperature at which ε_r of the ceramics begins to follow Curie-Weiss law. A lower T_0 than T_c means that the ferroelectric-paraelectric phase transition of the ceramic is a first-order phase transition. In Fig. S3d, the C is between 4.96×10^5 and 5.77×10^5, which means the samples are displacive-type ferroelectric. The P_s originates from the deviation of the atom from its equilibrium position in the paraelectric phase. To further investigate the relaxation feature, the degree of diffuseness (γ) is calculated by the following equation[5, 6]:

$$\frac{1}{\varepsilon_r} - \frac{1}{\varepsilon_m} = \frac{(T-T_m)^\gamma}{C} \tag{S4}$$

where ε_m denotes the dielectric constant at T_m. The relationship between $\ln(1/\varepsilon_r - 1/\varepsilon_m)$ and $\ln(T-T_m)$ is shown in Fig. S3c. In Fig. S3d and S3f, the γ (1.62~1.68) has the same trend with the ΔT_m (9~14 °C), proving that Li$^+$-ion doping does not significantly change the relaxation degree of the xLi-PNNZNZT.
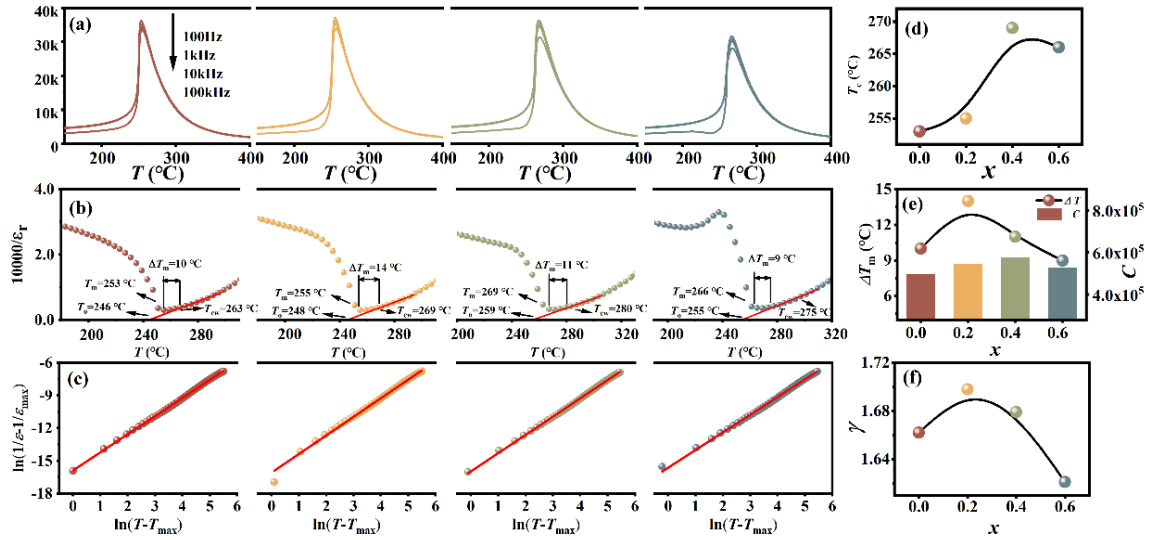
Fig. S3 (a) ε_r–T (150—400 °C), (b) $10000/\varepsilon_r$–T, (c) $\ln(1/\varepsilon_r - 1/\varepsilon_m)$ –$\ln(T-T_m)$ curves of the xLi-PNNZNZT. (d) T_C, (e) ΔT_m and C, (f) γ of the xLi-PNNZNZT.
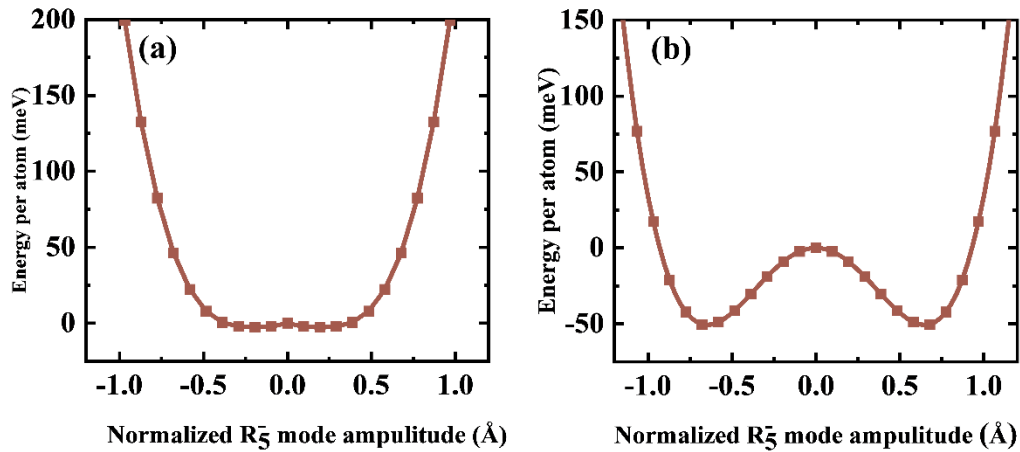

Fig. S4 The normalized R$^-_5$ mode that forms the antiphase oxygen octahedral tilt of (a) 0Li-PNNZNZT and (b) 0.4Li-PNNZNZT by DFT.
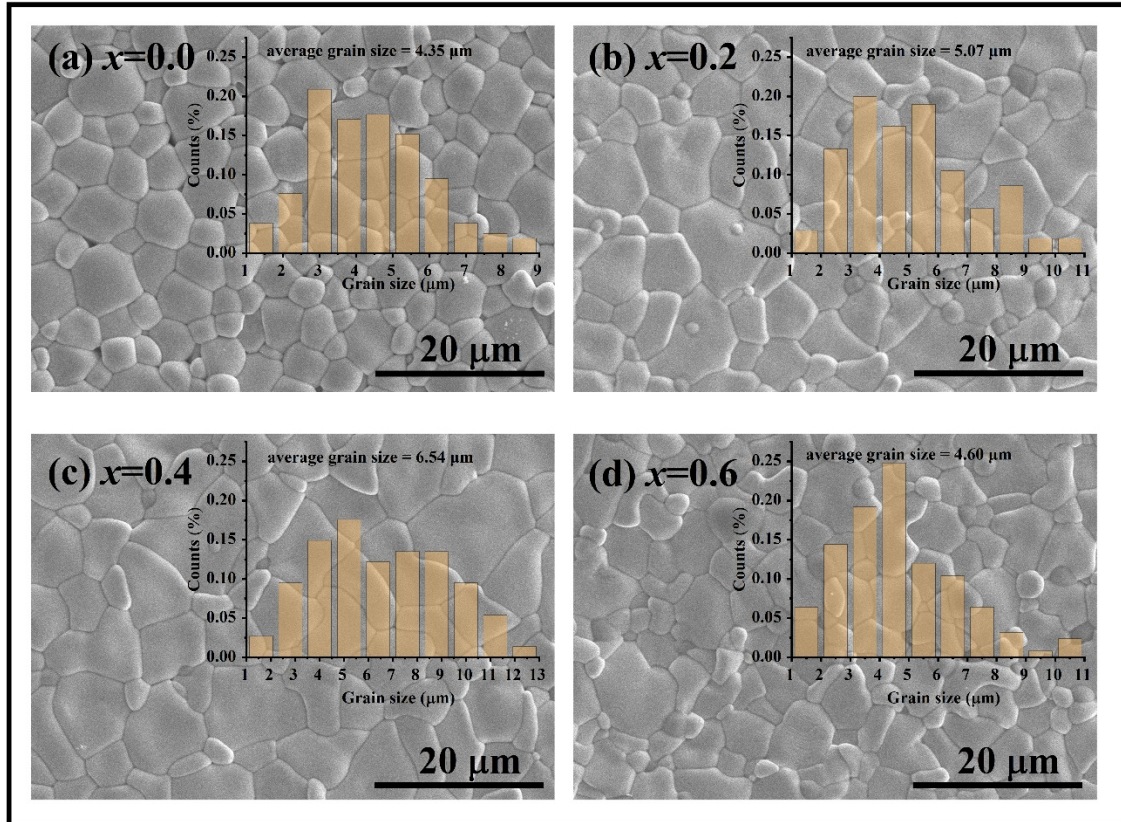
Fig. S5 (a-d) Surface SEM images and the grain size distribution of the xLi-PNNZNZT

Note that the V_0^+ is the switching voltage when DC voltage changes from negative to positive, and the V_0^- is the switching voltage when DC voltage changes from positive to negative values7. In Fig. S6a, the values of V_0^+ of the ceramics with x=0.0, 0.4, and 0.6 are mostly around 3.5-4.5 V, 2.5-3.5 V, and 2.5-4.0 V, respectively. And in Fig. S6b, the values of V_0^- of the ceramics with x=0.0, 0.4, 0.6 are mostly around (-3)-(-5) V, (-1)-(-4) V, (-2)-(-5) V, respectively. The V_0^+ and V_0^- of the ceramics reach the minimum values at x=0.4.
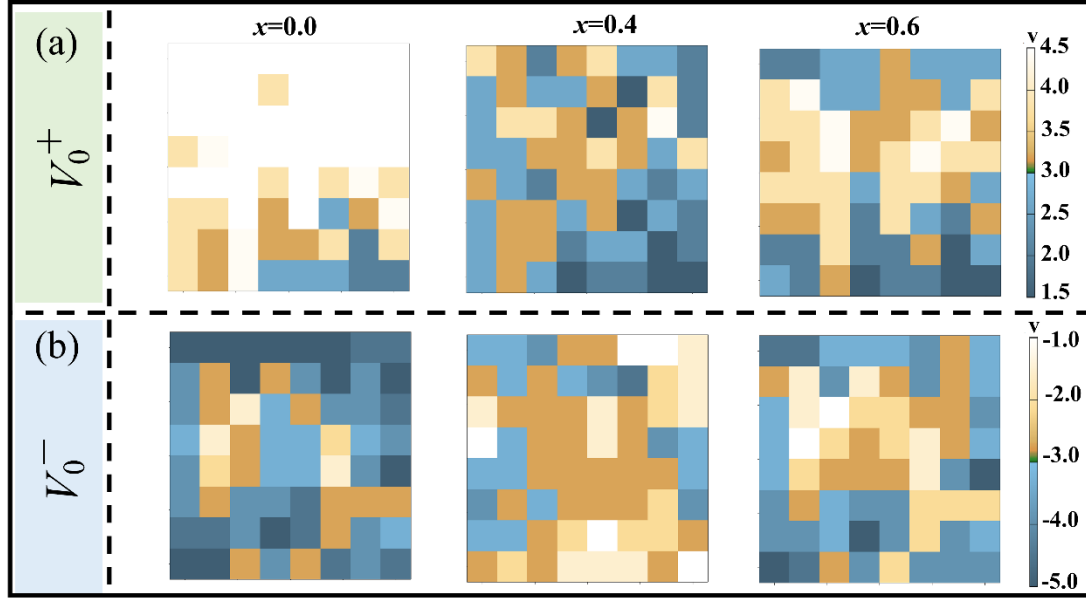
Fig. S6 shows the maps of switching parameters of xLi-PNNZNZT ceramics obtained using SS-PFM: (a) Positive coercive bias V_0^+, (b) Negative coercive bias V_0^-.

Fig. S7a shows the polarization–electric field (P–E) loops for the ceramics measured at different temperatures (30 °C—150 °C). As shown in Fig. S7d, the xLi-PNNZNZT ceramics have a maximum value of 34.27 μC/cm² of remnant polarization (P_r) and a minimum value of 8.96 kV/mm of coercive field (E_c).

As shown in Fig. S7b, the values of P_r and P_s of the ceramics gradually decrease with the increase in temperature. To further understand the law of domain motion, the relation between the back-switched polarization (P_{bc}) ($P_{bc}=P_s-P_r$) and the activation energy for domain wall movement (E_a) can be described as the following formula:[7]

$$P_{bc}=P_0\exp(-E_a/k_BT) \tag{S5}$$

where P_0 denotes a fitting constant; k_B and T express the Boltzmann constant and the absolute temperature, respectively. According to **equation** S5, the $\ln(P_{bc})$–1000/T curves of the ceramics are exhibited in Fig. S7c, and the value of E_a is obtained by the fitting. As observed in Fig. S7f, the E_a decreases from 0.0939 eV to 0.0456 eV with x

increasing from 0.0 to 0.4.
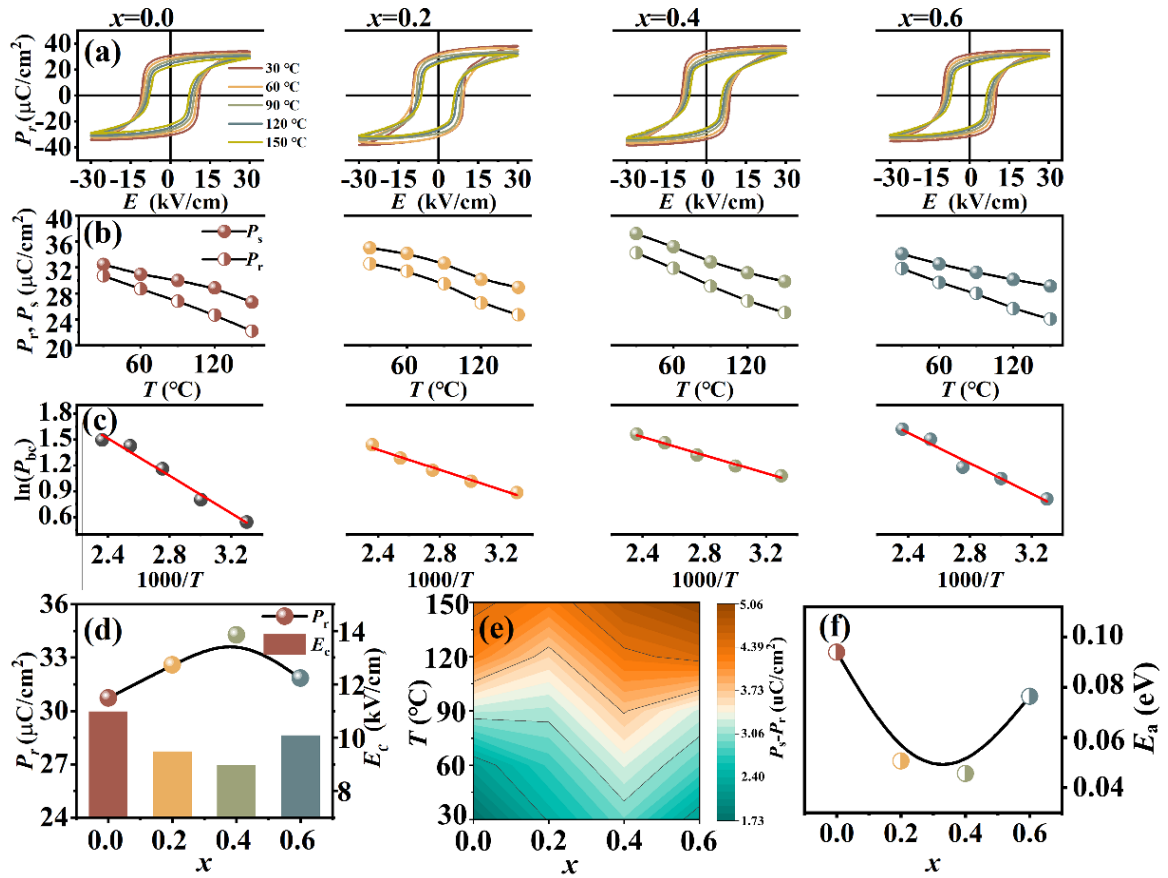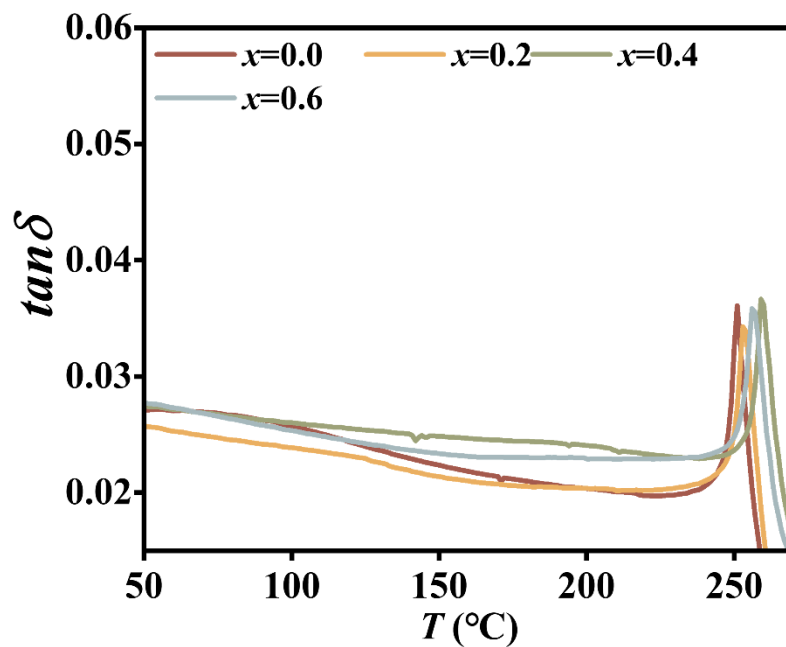

Fig. S7 (a) P–E loops, (b) P_r–T, P_s–T, (c) $\ln(P_{bc})$ –1000/T curves of the xLi-PNNZNZT

ceramics. (d) P_r and E_c (30°C), (e) P_s-P_r (30-150°C), (f) E_a as a function of x.
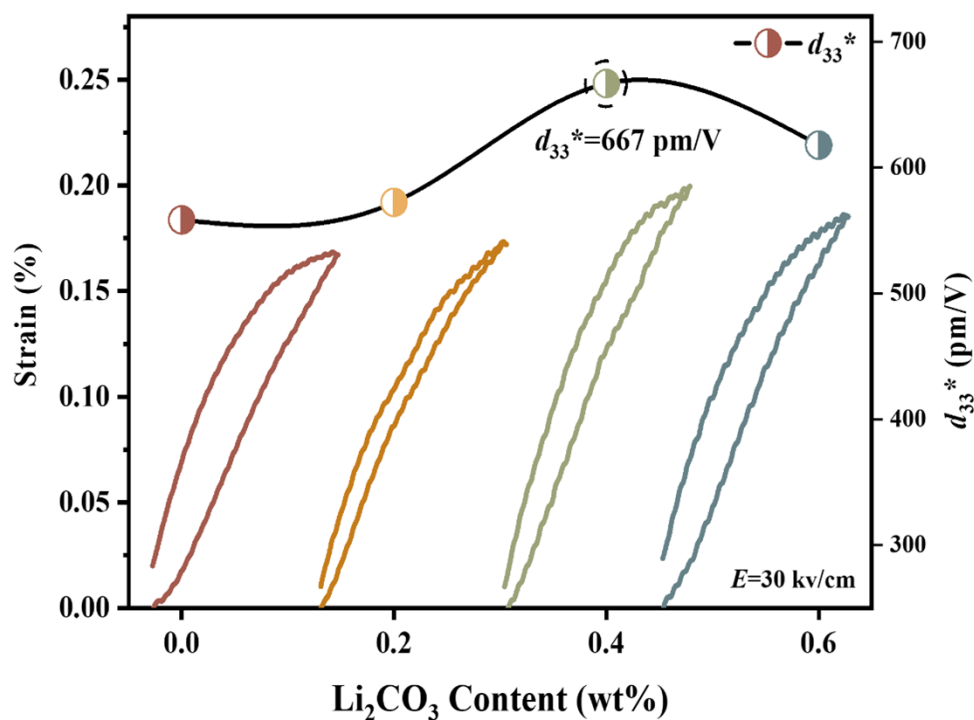
Fig. S8 The unipolar strain of xLi-PNNZNZT ceramics.

Fig. S9 Temperature dependence of the dielectric loss for the xLi-PNNZNZT ceramics at 10 kHz.

Table S1 Crystal structure parameters of the xLi-PNNZNZT derived from the Rietveld structure refinement program.

	x=0		x=0.2		x=0.4		x=0.6	
R_w (%)	7.66		8.06		7.47		7.42	
Sig	1.96		1.97		1.99		1.92	
symmetry	R phase	T phase	R phase	T phase	R phase	T phase	R phase	T phase
proportion	21.01	78.99	16.15	83.85	15.52	84.48	10.70	89.30
space group	R3m	P4mm	R3m	P4mm	R3m	P4mm	R3m	P4mm
a (Å)	4.0540	4.0297	4.0538	4.0276	4.0533	4.0274	4.0518	4.0269
b (Å)	4.0540	4.0297	4.0538	4.0276	4.0533	4.0274	4.0518	4.0269
c (Å)	4.0540	4.0890	4.0538	4.0888	4.0533	4.0887	4.0518	4.0886
α (deg)	89.7036	90.0000	89.6471	90.0000	89.7396	90.0000	89.7576	90.0000
V (Å³)	66.62	66.40	66.61	66.33	66.59	66.31	66.52	66.31
c/a	1.0000	1.0147	1.0000	1.0152	1.0000	1.0153	1.0000	1.0153

Table S2 Dielectric loss (tanδ) of the xLi-PNNZNZT ceramics measured at different temperatures and at 10 kHz.

x	tanδ@ RT	tanδ@ 50 °C	tanδ@ 100 °C	tanδ@ 150 °C	tanδ@ 200 °C	tanδ@ 250 °C
0.0	0.0253	0.0271	0.0257	0.0224	0.0204	0.0325
0.2	0.0254	0.0257	0.0239	0.0214	0.0204	0.0251
0.4	0.0261	0.0274	0.0260	0.0249	0.0241	0.0237
0.6	0.0264	0.0277	0.0253	0.0234	0.0229	0.0248

Table S3 The equation and diffusive coefficient of the xLi-PNNZNZT fitted by the modified Curie−Weiss law.

	The fitting equation	r
x=0.0	y=1.66212x-15.88152	1.662
x=0.2	y=1.69843x-16.08185	1.698
x=0.4	y=1.67948x-15.97479	1.679
x=0.6	y=1.62074x-15.63058	1.621

1. S.-H. Lee, H. M. Jang, H. H. Sung and H. Yi, 2002, *Appl. Phys. Lett.,* **81**, 2439–2441.

2. R. Nie, Q. Zhang, Y. Yue, H. Liu, Y. Chen, Q. Chen, J. Zhu, P. Yu and D. Xiao, *J. Appl. Phys.*, 2016, **119**, 124111.

3. H.-W. Zhu, D.-Y. Zheng, X.-J. Wang, L. Yang, C. Fang and Z.-H. Peng, *J. Mater. Sci.: Mater. Electron.*, 2018, **29**, 16864–16871.

4. H. Chen, J. Xing, J. Xi, T. Pu, H. Liu and J. Zhu, *J. Am. Ceram. Soc.*, 2021, **104**, 6266–6276.

5. B. Wu, C. Zhao, Y. Huang, J. Yin, W. Wu and J. Wu, *ACS Appl. Mater. Interfaces*, 2020, **12**, 25050–25057.

6. Y. Yue, Q. Zhang, R. Nie, P. Yu, Q. Chen, H. Liu, J. Zhu, D. Xiao and H. Song, *Mater. Res. Bull.*, 2017, **92**, 123–128.

7.   B. Ma, Z. Hu, S. Liu, M. Narayanan and U. Balachandran, *Appl. Phys. Lett.*, 2013, **102**,072901.